THE JOURNAL OF BIOLOGICAL CHEMISTRY VOL. 281, NO. 36, pp. 26289–26297, September 8, 2006
Printed in the U.S.A.

The Structural Basis for Substrate Anchoring, Active Site Selectivity, and Product Formation by P450 PikC from *Streptomyces venezuelae*[*] [S]

Received for publication, June 7, 2006, and in revised form, June 30, 2006 Published, JBC Papers in Press, July 6, 2006, DOI 10.1074/jbc.M605478200

David H. Sherman[‡1], Shengying Li[‡], Liudmila V. Yermalitskaya[§], Youngchang Kim[¶], Jarrod A. Smith[§], Michael R. Waterman[§], and Larissa M. Podust[§2]

From the [‡]Life Sciences Institute and Department of Medicinal Chemistry, University of Michigan, Ann Arbor, Michigan, 48109, the [§]Department of Biochemistry and Center in Structural Biology, Vanderbilt University School of Medicine, Nashville, Tennessee, 37232, and the [¶]Argonne National Laboratory, Structural Biology Center, Argonne, Illinois, 60439

The pikromycin (Pik)/methymycin biosynthetic pathway of *Streptomyces venezuelae* represents a valuable system for dissecting the fundamental mechanisms of modular polyketide biosynthesis, aminodeoxysugar assembly, glycosyltransfer, and hydroxylation leading to the production of a series of macrolide antibiotics, including the natural ketolides narbomycin and pikromycin. In this study, we describe four x-ray crystal structures and allied functional studies for PikC, the remarkable P450 monooxygenase responsible for production of a number of related macrolide products from the Pik pathway. The results provide important new insights into the structural basis for the C10/C12 and C12/C14 hydroxylation patterns for the 12- (YC-17) and 14-membered ring (narbomycin) macrolides, respectively. This includes two different ligand-free structures in an asymmetric unit (resolution 2.1 Å) and two co-crystal structures with bound endogenous substrates YC-17 (resolution 2.35 Å) or narbomycin (resolution 1.7 Å). A central feature of the enzyme-substrate interaction involves anchoring of the desosamine residue in two alternative binding pockets based on a series of distinct amino acid residues that form a salt bridge and a hydrogen-bonding network with the deoxysugar C3′ dimethylamino group. Functional significance of the salt bridge was corroborated by site-directed mutagenesis that revealed a key role for Glu-94 in YC-17 binding and Glu-85 for narbomycin binding. Taken together, the x-ray structure analysis, site-directed mutagenesis, and corresponding product distribution studies reveal that PikC substrate tolerance and product diversity result from a combination of alternative anchoring modes rather than an induced fit mechanism.

Macrolide antibiotics comprise a large group of medicinal agents characterized by a macrocyclic lactone ring, to which one or more sugar residues are covalently linked. Despite considerable structural variation, macrolides represent a homogeneous group of therapeutic drugs with similar activity spectra and mode of action as anti-infective agents. The success of macrolide antibiotics is attributed to their propensity to bind to the large subunit of prokaryotic ribosomes and inhibit protein synthesis, thereby preventing bacterial growth (1, 2). The first generation macrolide introduced into clinical practice over 50 years ago was erythromycin. Since then, macrolide antibiotics have been further optimized, resulting in improved 14-, 15-, and 16-membered ring macrolides (second generation), acylides, and ketolides (third generation) (3).

Most of the natural product macrolide antibiotics are produced by *Streptomyces* sp. and related bacteria, in which assembly of polyketides from simple carboxylic acid precursors is catalyzed by modular polyketide synthases. Over the past 15 years, advances in understanding the modular architecture of polyketide biosynthetic machinery has enabled development of metabolic engineering approaches for production of new antibiotics (4–7). However, significant additional structural variability of polyketide-derived natural products is due to post-polyketide synthase biosynthetic modifications that typically include hydroxylation/epoxidation and/or glycosylation. In most antibiotic biosynthetic pathways, hydroxylation(s) occur(s) at the late stages of assembly after formation of the natural product scaffold and often after glycosylation events. Such modifications are often necessary to impart or enhance biological activity (8). The 3-(dimethylamino)-3,4,6-trideoxy sugar desosamine (or mycaminose) confers biological activity to a number of macrolide antibiotics such as erythromycin, troleandomycin, mycinamicin, megalomicin (desosamine), tylosin, carbomycin, and spiramycin (mycaminose) and is the only glycoside present on pikromycin, methymycin, and the highly potent semisynthetic ketolide telithromycin (9).

Both macrolides and ketolides were shown crystallographically to bind in a specific pocket in the ribosomal tunnel via interactions with 23 S rRNA and act to block sterically egress of the nascent protein chains (10). The desosamine sugar (or mycaminose) attached to C5 of the 14-, 15-, and 16-membered ring macrolactones extends up the tunnel toward the peptidyl transferase center. Interactions between desosamine and the

* This work was supported by National Institutes of Health Grants GM37942, GM69970, ES00627 (to M. R. W.), and GM078553 (to D. H. S.), by grants from the Vanderbilt-Meharry Center for AIDS Research, Vanderbilt University Medical Center (VUMC) Discovery Grant Program, and U. S. Civilian Research and Development Foundation (to L. M. P.). The costs of publication of this article were defrayed in part by the payment of page charges. This article must therefore be hereby marked "*advertisement*" in accordance with 18 U.S.C. Section 1734 solely to indicate this fact.

The atomic coordinates and structure factors (code 2BVJ, 2C7X, and 2C6H) have been deposited in the Protein Data Bank, Research Collaboratory for Structural Bioinformatics, Rutgers University, New Brunswick, NJ (http://www.rcsb.org/).

[S] The on-line version of this article (available at http://www.jbc.org) contains two supplemental movies.

[1] To whom correspondence may be addressed. Tel.: 734-615-9907; Fax: 734-615-3641; E-mail: davidhs@umich.edu.

[2] To whom correspondence may be addressed. Tel.: 615-343-0943; Fax: 615-322-4349; E-mail: larissa.m.podust@vanderbilt.edu.

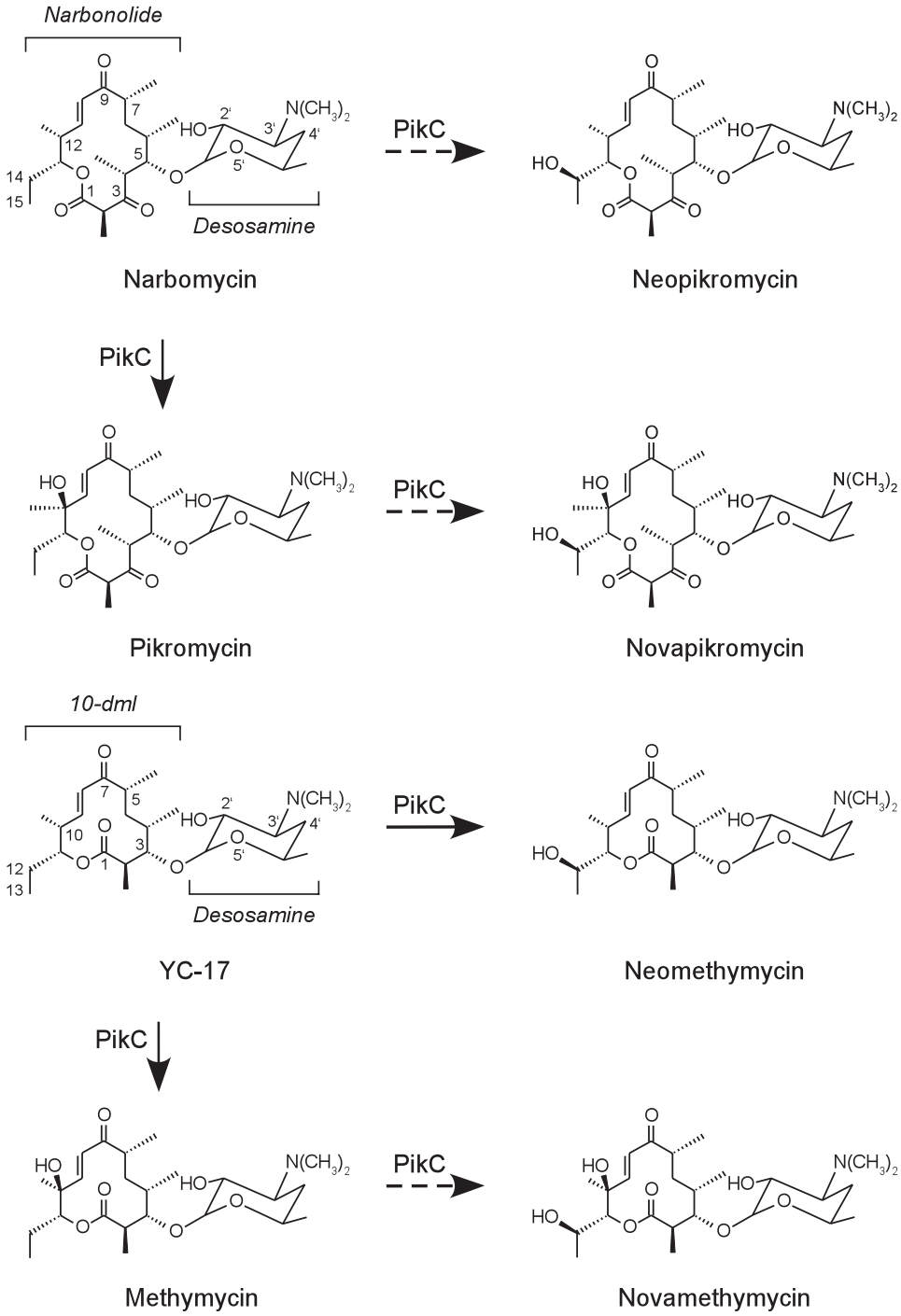

FIGURE 1. **Catalytic roles of PikC.** Hydroxylated natural products obtained from the Pik pathway are shown. *10-dml*, 10-deoxymethynolide. *Solid arrows* indicate reactions leading to the primary products.

ribosome play a key role in both macrolide selectivity and macrolide resistance (11).

Previous studies have shown that metabolic engineering approaches can provide structurally variable macrolactones (12, 13) and/or extend a repertoire of deoxysugars coupled to macrolide aglycones (14–18). The Pik[3] biosynthetic gene cluster of *Streptomyces venezuelae* represents an effective system for the synthesis of novel polyketide antibiotics due to (i) its ability to generate two macrolactone ring systems; (ii) the presence of a flexible desosaminyl transferase (DesVII) that is tolerant of changes in macrolactone structure (13, 18, 19), as well as modifications to the sugar substituent (14-17); and finally, (iii) the unusual P450 monooxygenase (CYP) PikC (CYP107L1), responsible for the diverse pattern of hydroxylated natural products obtained from the Pik pathway (Fig. 1).

A series of particularly intriguing observations were made several years ago regarding the substrate selectivity of PikC that appeared to correlate directly with hydrogen bond functionality at the C3′ position of the glycoside, with no tolerance for modifications at C4′ (14–17). Such a stringent requirement toward sugar structure contrasts with the apparent flexibility of PikC toward the macrolactone core of a substrate. Thus, PikC is able to catalyze mono-hydroxylation at either C10 or C12 of the 12-membered ring macrolactone of YC-17, giving rise to methymycin and neomethymycin, respectively, as well as at C12 of the 14-membered ring of narbomycin, giving rise to pikromycin (20). Hydroxylation at the C14 position of pikromycin, giving rise to neopikromycin, occurs with a very low yield, which precluded isolation and characterization of this metabolite until recently (21). Dihydroxylation of YC-17 results in novamethymycin (Fig. 1), a product that is found in small quantities *in vivo* and appears to be converted from methymycin *in vitro* (22). Dihydroxylation of narbomycin results in a very low but detectable production of novapikromycin (21).

Here we provide new information regarding the diverse hydroxylation pattern of the PikC monooxygenase by determining its crystal structure in a variety of forms, including ligand-free and bound to endogenous substrates YC-17 and narbomycin (see Table 1). This series of crystal structures has revealed that in the absence of a substrate, PikC adopts both "open" and "closed" conformations due to repositioning of the BC-loop and the F and G helices. This dynamic process appears to enable substrate access to the active site; however, it does not account for PikC substrate flexibility, which is largely due to the

[3] The abbreviations used are: Pik, pikromycin; r.m.s., root mean square; MES, 4-morpholineethanesulfonic acid.

TABLE 1
Data collection and refinement statistics
PEG, polyethylene glycol; MME, monomethyl ether.

PDB ID	Ligand-free 2BVJ	Narbomycin-bound 2C7X	YC-17-bound 2C6H
Data collection			
Resolution, Å	2.10	1.70	2.35
Wavelength, Å	1.00000	0.97918	1.72196
Space group	C2	$P2_12_12_1$	$P2_12_12_1$
Cell dimensions			
a, *b*, *c*, Å	218.2, 64.2, 73.6	59.0, 64.9, 92.8	60.5, 104.7, 153.6
α, β, γ, °	90.00, 107.15, 90.00	90.00, 90.00, 90.00	90.00, 90.00, 90.00
Molecules in an asymmetric unit	2	1	2
Solvent content, %	52	34	52
R_{sym}[a,b], %	6.0 (26.0)	5.9 (37.3)	10.0 (49.0)
I/σ	19.5 (3.7)	65.3 (3.6)	23.8 (4.3)
Unique reflections	55910	35331	33864
Completeness, %	98.2 (87.6)	97.3 (80.9)	98.3 (95.8)
Redundancy	3.7 (3.1)	11.2 (6.5)	6.8 (6.2)
Crystallization conditions	10% PEG 8000, 0.1 M HEPES, 7.5	0.8 M $(NH_4)_2SO_4$, 0.1 M MES, 6.0	30% PEG MME 5000, 0.2 M $(NH_4)_2SO_4$, 0.1 M MES, 6.5
Refinement			
Reflections used in refinement	53812	34218	72999
R_{crys}/R_{free}[c], %	20.2/24.3	20.7/23.2	19.5/23.1
No. atoms			
Protein	6046	3212	6101
Heme	86	43	86
Substrate	0	36	64
Water/ion	317/16	171/0	216/25
Wilson plot *B*-values, Å^2	13.2	28.6	20.5
Mean *B*-factors, Å^2			
Protein	28.3	35.9	23.2
Heme	17.7	23.2	14.6
Substrate	NA	45.1	20.12
Water	30.3	41.9	23.9
r.m.s. deviations			
Bond lengths, Å	0.006	0.01	0.006
Bond angles, °	1.2	1.4	1.2
Ramachandran[d]	A, 89.6/10.4; B, 90.9/9.1	A, 92.3/7.4/0.3	A, 91.1/8.9; B, 92.6/7.4

[a] $R_{sym} = \Sigma|I_i - \langle I\rangle|/\Sigma I_i$, where I_i is the intensity of the *i*th observation, and $\langle I\rangle$ is the mean intensity of reflection.
[b] Numbers in parentheses correspond to the highest resolution shell.
[c] $R_{cryst} = \Sigma\,||F_o| - |F_c||/\Sigma\,|F_o|$, calculated with the working reflection set. R_{free} is the same as R_{cryst} but calculated with the reserved reflection set.
[d] Program PROCHECK (28).

combination of a single macrolactone binding site with two alternative desosamine binding pockets. In both pockets, the desosamine C3′ dimethylamino group is sandwiched between two carboxyl-containing (Glu, Asp) amino acids found in the BC-region, forming a salt bridge to the more proximal carboxyl group. Site-directed mutagenesis revealed that formation of this salt bridge is essential for PikC function.

EXPERIMENTAL PROCEDURES

Expression and Purification of PikC—The PikC expression vector (20) was used for site-directed mutagenesis according to the QuikChange (Stratagene) protocol and for protein expression. The desired mutations were confirmed by DNA sequencing. Proteins were expressed in HMS174(DE3) *Escherichia coli* strain at 20 °C with an induction period of 20 h. Purification on nickel-nitrilotriacetic acid resin (Qiagen) was followed by flow-through chromatography on S-Sepharose (Amersham Biosciences) and binding to Q-Sepharose (Amersham Biosciences), from which PikC was eluted by a NaCl gradient, 0–0.5 M. Protein was concentrated to 1 mM by using a Centriprep concentrating device. Quality and quantity of purified protein were accessed by SDS-PAGE and CO-reduced difference spectra (23).

Crystallization and Diffraction Data Collection—Purified PikC with the His tag at 0.2 mM concentration was either subjected to crystallization alone or mixed with substrate at 2 mM concentration (1:10 ratio) and then subjected to crystallization. In all cases, prior to crystallization, the protein was incubated for 1 h on ice with 1 mM dithiothreitol to prevent dimerization via Cys-375, which is readily observed during prolonged storage of PikC. Co-crystallization with ligands, either inhibitor or substrates, resulted in crystals of different size and morphology grown by vapor diffusion hanging drop method from a variety of crystallization conditions as indicated in Table 1. Ligand-free PikC crystals grew in the presence of 5 mM azole inhibitor 4-phenylimidazole (not found in the final crystal structure). All diffraction data were collected at 100–110 K at the Southeast Regional Collaborative Access Team (SER-CAT) 22ID and Structural Biology Center 19ID beamlines, Advanced Photon Source, Argonne National Laboratory, Argonne, IL. Glycerol mixed with the reservoir solution was used as a cryoprotectant at concentrations ranging from 18 to 25%, which have been determined empirically for each crystal type. The images were integrated and the intensities were merged by using HKL2000 (24).

Crystal Structure Determination—Molecular replacement was used to determine all crystal structures (Table 1). The ligand-free form of PikC was initially determined using the program CNS (25) and EryF (46% sequence identity) coordinates

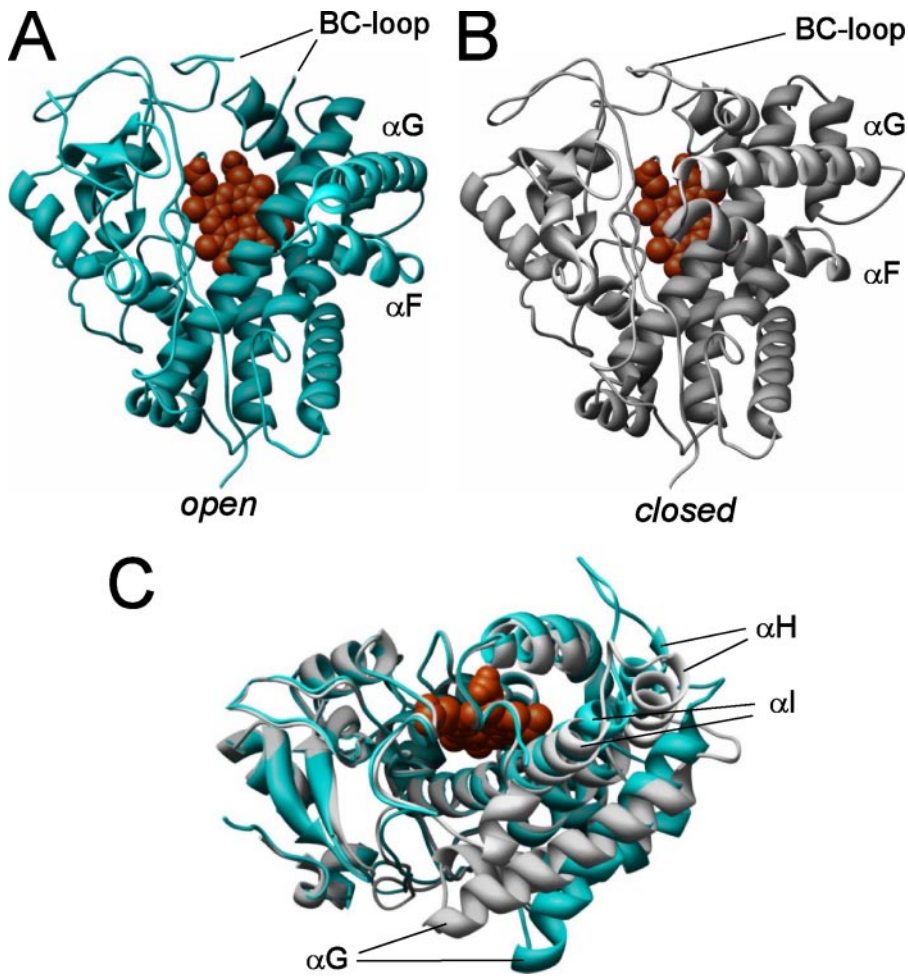

FIGURE 2. **Ribbon representation of ligand-free PikC.** *A*, open, and *B*, closed conformations of ligand-free PikC (2BVJ). *C*, overlay of both conformations, open (*cyan*) and closed (*gray*), demonstrating that in the open form, the F and G helix are bent away from the heme to enable substrate access to the active site. Molecules in *C* are rotated ~90° toward the viewer along a horizontal axis in the plane of drawing when compared with *A* and *B*. The F helix is not seen in this orientation. Closed conformation is related within r.m.s. deviations of 0.58 Å for Cα atoms to catalytically relevant YC-17- and narbomycin-bound forms. The heme co-factor is shown in *red*.

(26) as a search model. Crystal structures of YC-17- and narbomycin-bound PikC were similarly determined by molecular replacement using CNS (25), with ligand-free PikC coordinates as a search model. All reflections were used for refinement. The final atomic models (Table 1) were obtained after a number of iterations of refinement (CNS (25)) and manual model building with the program O (27). Ramachandran statistics (28) (Table 1) indicate no outliers with an exception of one residue, Pro-181, in the narbomycin-bound PikC structure (Protein Data Bank ID 2C7X). From 10 to 13 N-terminal residues, depending on the crystal form, are missing in all protein chains due to insufficient electron density in this region. Also, six BC-loop residues are missing in an open ligand-free form due to the same reason.

PikC Product Profile Analysis—The enzymatic conversions of YC-17 or narbomycin *in vitro* were carried out using a previously developed assay (20). The standard reaction contained 1 μM PikC (native enzyme or mutants), 0.5 mM YC-17 or narbomycin, 3.5 μM spinach ferredoxin, 0.01 units of spinach ferredoxin-$NADP^+$ reductase, and 1 mM NADPH in 200 μl of 50 mM Na-PO_4 (pH 7.3), 1 mM EDTA, 0.2 mM dithiothreitol, 10% (v/v) glycerol. The reaction was terminated after 40 min of incubation at 30 °C by the addition of 300 μl of chloroform, and products were subsequently extracted, dried, dissolved in 120 μl of methanol, and analyzed by reverse-phase (C18) high pressure liquid chromatography (Waters Corp., Milford, MA) by using a linear gradient (0–100%) of water:trifluoroacetic acid:triethylamine(99.8:0.1:0.1)/acetonitrile:trifluoroacetic acid:triethylamine (99.8:0.1:0.1) as a mobile phase at the flow rate of 1.0 ml/min.

RESULTS AND DISCUSSION

Ligand-free PikC—The crystal structure of the ligand-free form of PikC revealed that two molecules in an asymmetric unit adopt two different conformations, referred to as open and closed depending on the position of the F and G helices and the BC-loop, the latter being partially disordered in the open conformation (Fig. 2). These regions are generally flexible in P450s and readily reposition in response to inhibitor or substrate binding in the active site (29–31). To our knowledge, this is the first time that a P450 demonstrates such protein dynamics (linear repositioning of the FG-loop in the ligand-free PikC is within 12 Å) in the absence of a bound ligand, probably as a result of natural motions (supplemental movies 1 and 2), although the first structural indications of open/close differences in the FG-region were noticed for a ligand-free P450BM3 (32). The most compelling need for such protein dynamics is to allow substrate access to the active site and subsequent product release. A water molecule is bound as the sixth ligand to the hexa-coordinated heme Fe^{3+} atom. Scattered electron density accommodates a few additional water molecules that together form a hydrogen bond network within the active site. Water molecules are displaced upon substrate binding.

X-ray Structure of Narbomycin-bound PikC—The 14-membered ring macrolide narbomycin is one of the two endogenous substrates for PikC (20). Hydroxylation of narbomycin at C12 (Fig. 1) of the macrolactone ring gives rise to the antibiotic pikromycin. In the co-crystal structure (1.75 Å resolution), narbomycin is unambiguously positioned in the active site, and its electron density is well defined (Fig. 3*A*). Of particular significance are interactions between the C3′ dimethylamino group of the desosamine sugar and two carboxyl-containing residues localized in the BC-region (Glu-85 and Asp-50) (Fig. 4*A*). Although proximal Glu-85 (3.2 Å distance) provides a salt bridge contact, distal Asp-50 (5.3 Å distance) may compensate

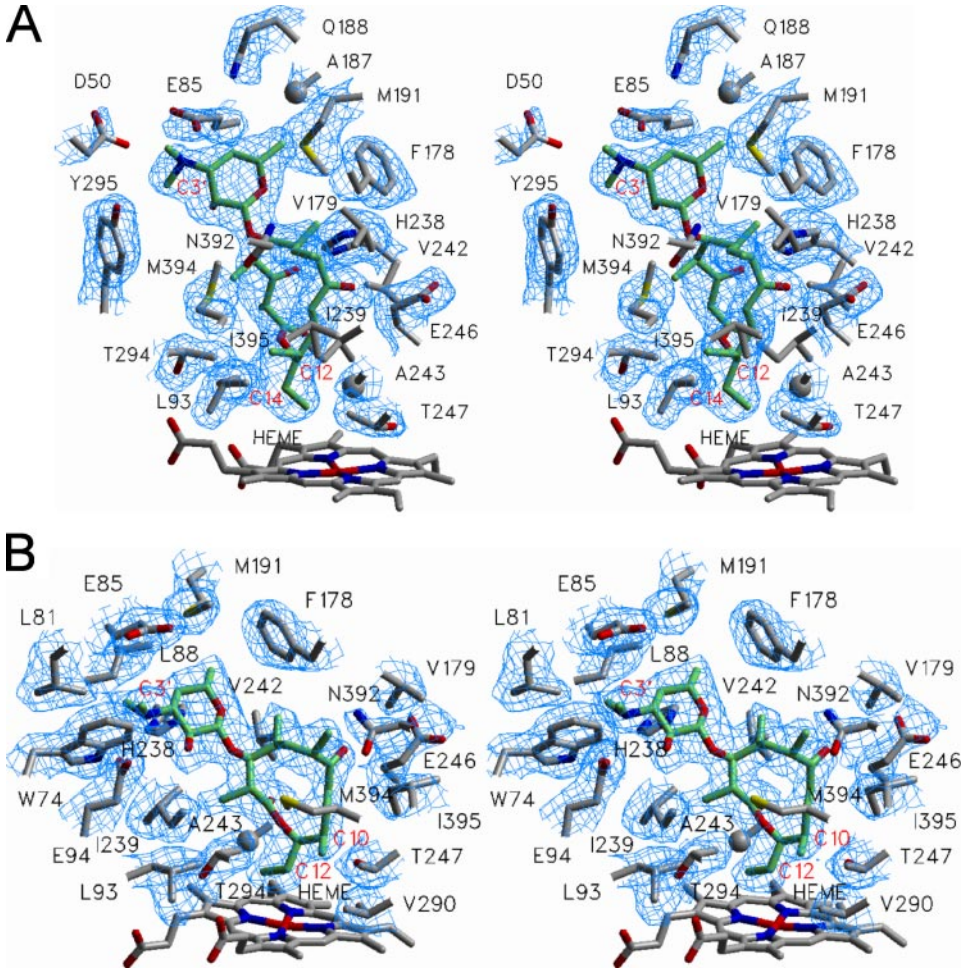

FIGURE 3. **Substrate binding in the PikC active site.** Stereo views of narbomycin (2C7X) (*A*) and YC-17 (2C6H) (*B*) bound in the active site of PikC are shown. Amino acid residues within 4.0 Å (labeled in *black*) are also shown. Carbon atoms are labeled in *red*. Fragments of $2F_o - F_c$ electron density composite omit map contoured at 0.8 σ are in *blue*. To avoid excessive cluttering of stereo views with the electron density bulks, a number of residues, including heme and those that project on top of the substrate or each other, are excluded from the map calculation. Excluded in addition to heme in *panel A* are: Val-179, Ile-239, Val-242, Asn-392, and Ile-395; Excluded in addition to heme in *panel B* are: His-238, Val-242, Ala-243, and Met-394.

for a partial positive charge of the protonated tertiary amine. A calculated pK_a of 8.85 for the desosamine nitrogen atom (calculated by using the on-line program SPARC (33)) is in good agreement with the values experimentally obtained for erythromycin (34), suggesting that at neutral pH, desosamine exists primarily in the protonated form. Interestingly, electrostatic interactions involving the C3′ dimethylamino group are also involved in macrolide recognition in the ribosome tunnel where a positive charge is neutralized by a negative charge of an rRNA phosphate group invariantly positioned within 5 Å in structurally defined macrolide/ribosome complexes (35–38); however, no salt bridge is formed (Fig. 4*C*). In this regard, macrolide resistance in bacterial pathogens is often attributed to mono- or dimethylation at the A2058 N6 position (*E. coli* numbering) or to mutations that change nucleotide identity, both eliminating interactions with desosamine (11). In addition, PikC amino acid side chains Phe-178, Ala-187, Gln-188, Met-191, and Tyr-295 are within 4 Å of the desosamine moiety (Figs. 3*A* and 4*A*). Although substrate anchoring by a biosynthetic P450 involving desosamine is unique, another type of anchoring mechanism was observed previously for the epothilone P450 EpoK from *Sorangium cellulosum*. In EpoK, a pendant thiazole moiety linked to the macrolactone ring system is involved in π-π interactions with two aromatic amino acids that determine substrate specificity (39).

Significantly, the macrolactone ring of narbomycin is bound almost entirely via hydrophobic interactions with amino acid side chains Leu-93, Phe-178, Val-179, Ile-239, Val-242, Ala-243, Thr-247, Thr-294, Met-394, and Ile-395 plus three hydrophilic ones, Glu-246, His-238, and Asn-392, but no hydrogen bonding is involved. The Thr-247 hydroxyl is involved in hydrogen bonding with the I helix main chain atoms, causing a local distortion observed in many if not all structurally defined P450s. The Glu-246 side chain is in a conformation that is flipped away from the substrate (Fig. 3*A*). These two I helix residues, Glu-246 and Thr-247, are highly conserved among P450s and play an important part in activation and delivery of protons to the iron-linked dioxygen (40). Surprisingly, the allylic C12 carbon (analog of C10 in YC-17) is positioned 7.1 Å away from the heme iron, whereas the distance between methylene C14 carbon (analog of C12 in YC-17) and the heme iron is only 5.3 Å (Fig. 4*A*). Despite this distance differential that would appear to favor hydroxylation of the more proximal C14 atom, hydroxylation of narbomycin at this position occurs with very low yield (~40:1 ratio *in vivo*) (21). The structure suggests that unfavorable stereochemistry of the C–H bonds at C14 (pointing away from the oxygen scission site) is the basis for this, which could be due to rotation of the C14–C15 bond toward the heme iron, possibly to avoid steric interference with the side chains of amino acids Leu-93 and Thr-294 (Fig. 3*A*). In contrast, a C–H bond at C12 is positioned favorably toward the oxygen scission site. Whether hydroxylation is controlled by regio- and stereochemistry of the C–H bond, by distance to the heme iron, or by the iron-oxo reactive intermediate (or a combination of these variables) remains to be elucidated. It is also possible that Fe^{+3} reduction followed by oxygen binding might result in repositioning of narbomycin, as is indicated by NMR paramagnetic relaxation studies on the P450BM3-laurate complex, in which 6 Å movement of the substrate into the correct position for hydroxylation has been detected (41).

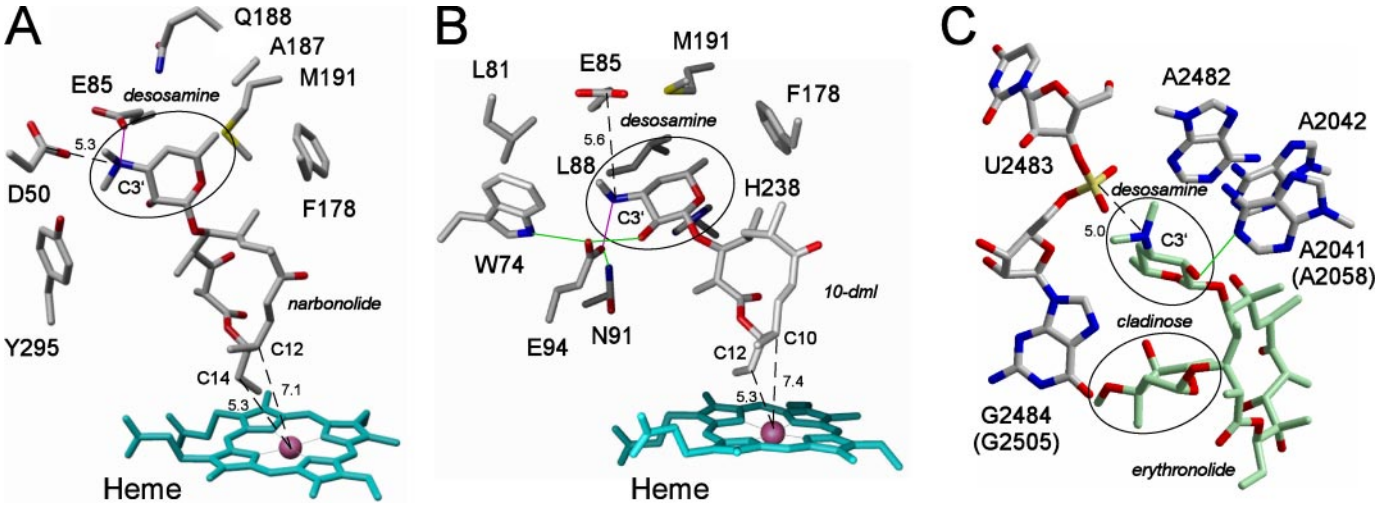

FIGURE 4. **Desosamine anchoring.** Desosamine interactions in narbomycin (*A*) and YC-17 (*B*) binding sites of PikC are shown. Amino acid residues within 4.0 Å from desosamine are also shown. *C*, erythromycin (in *green*) is shown bound to the large ribosomal subunit from eubacteria *Deinococcus radiodurans* (1JZY) (35). The phosphate group of G2484 (G2505) interacts with the dimethylamino group of desosamine. Nucleotide numbering according to the *E. coli* sequence is indicated by *parentheses*. Hydrogen bonds are highlighted in *green*, salt bridges are highlighted in *magenta*, and the distances are in Angstroms.

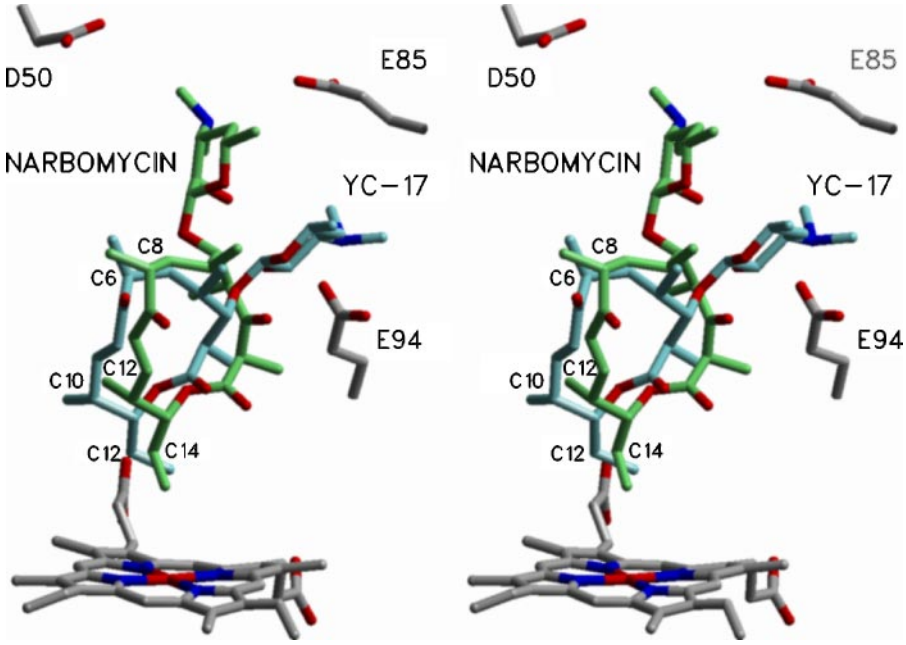

FIGURE 5. **Two desosamine anchoring modes in PikC.** A stereo view of overlaid YC-17 and narbomycin bound in the PikC active site is shown. Narbomycin is in *green*, and YC-17 is in *cyan*. The *S*-configuration observed for the C6 atom of YC-17 in the crystal structure conflicts with the *R*-configuration derived based on the methymycin, neomethymycin, narbomycin, and pikromycin structures (48–50). Formation of this unnatural stereoisomer may have been a result of adventitious epimerization at C6 via the enol intermediate during long term storage of 10-deoxymethynolide.

Alternatively, hydroxylation at the 7 Å remote allylic C12 atom in narbomycin may result from the iron-peroxo intermediate Fe^{+3}-OO^{-} (or its protonated form) as an "active oxygen" as opposed to a widely accepted P450 oxidant oxo-ferryl radical, compound I (42). This frequently discussed alternative pathway requires a homolytic O–O bond cleavage and is generally not thought to be involved in the normal monooxygenation process (43). Classical examples of the role of a nucleophilic iron-peroxo species in P450 catalysis are the oxidative decarbonylation of aldehydes and the final step of the aromatization reaction of androstenedione to estrone catalyzed by human aromatase (44). However, growing evidence supports the active role of peroxy-iron as an electrophilic oxidant in hydroxylation of C–H bonds in the hypersensitive cyclopropane probe (45) and epoxidation of olefins (46, 47). In narbomycin and YC-17, the allylic C–H bond is weaker than an alkanyl C–H by about 16 kcal/mol (42). In addition, the C10=C11 double bond in narbomycin and YC-17 is conjugated to the carbonyl group, which leads to a polarization of the double bond and draws electron density toward the oxygen atom away from the conjugated system. This serves to further weaken the allylic C–H bond, thus decreasing the barrier for its activation.

X-ray Structure of YC-17-bound PikC—The smaller 12-membered ring macrolide YC-17 is the second endogenous substrate of PikC (20). In contrast to narbomycin, it is hydroxylated *in vivo* and *in vitro* at two different positions (~1:1 ratio). Modification at allylic C10 results in methymycin, whereas modification at methylene C12 results in formation of neomethymycin (Fig. 1). In the co-crystal structure determined to 2.35 Å resolution, YC-17 is unambiguously positioned in one orientation within the active site, and its electron density is well defined (Fig. 3*B*). As observed with narbomycin, the macrolactone ring of YC-17 is bound almost entirely via hydrophobic interactions projecting the more hydrophilic surface of the lactone toward the I helix and is devoid of hydrogen bonding. The binding site for the 12-membered ring lactone overlaps the entire binding site for the 14-membered ring macrocycle plus an extra amino acid residue, Val-290. As observed for narbomycin, the C3′ dimethylamino group of the

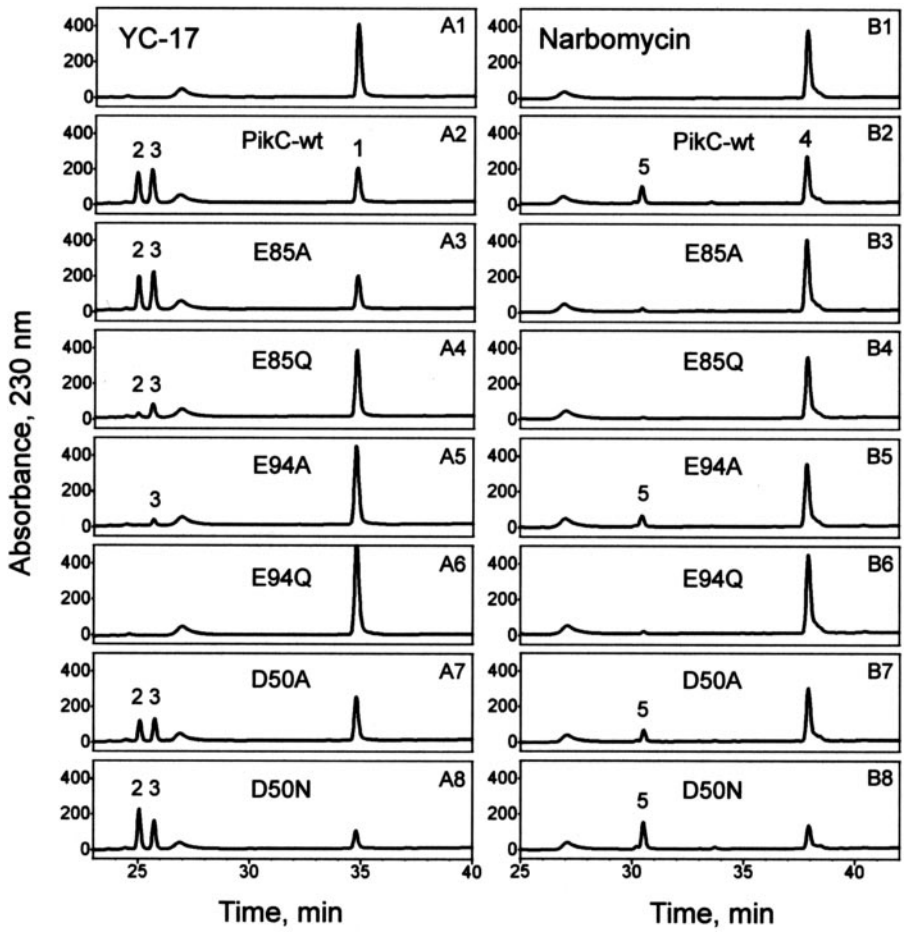

FIGURE 6. **Functional activity of PikC mutants.** High pressure liquid chromatography analyses of PikC-catalyzed reactions using YC-17 (*A series*) and narbomycin (*B series*) as substrate are shown. *A1/B1*, negative control in the absence of PikC. *A2/B2*, PikC wild type (*PikC-wt*). Mutants are used as indicated in the figure. Compound identities are as follows: ***1***, YC-17; ***2***, neomethymycin; ***3***, methymycin; ***4***, narbomycin; ***5***, pikromycin. Conversion of narbomycin at low efficiency is probably due to use of exogenous redox partners (*e.g.* spinach ferredoxin reductase) in P450 reconstitution assays.

desosamine moiety in YC-17 is sandwiched between two carboxyl groups (Glu-85 and Glu-94) in a different binding pocket (Fig. 5) that is more buried in the protein interior when compared with the narbomycin desosamine binding site (Figs. 3*B* and 4*B*). Although proximal Glu-94 (2.7 Å distance) provides a salt bridge, distal Glu-85 (5.8 Å distance) may potentially compensate for the partial positive charge at the desosamine tertiary amine. Trp-74, Asn-91, and Glu-94 participate in a network of hydrogen bond contacts with the desosamine moiety (Fig. 4*B*). The BC-loop is more extensively involved in interactions with desosamine in this binding pocket, providing additional hydrophobic contacts via Trp-74, Leu-81, and Leu-88. The remaining desosamine-protein interactions are via Met-191 and His-238. Interestingly, the desosamine interaction pattern with amino acid residues in the PikC active site mimics interactions of desosamine with the bacterial ribosome drug target, although these involve specific RNA nucleotides and the phosphate backbone (Fig. 4*C*).

Both YC-17- and narbomycin-bound PikC differ slightly (~2 Å) in positioning of the FG-region, which is most dynamic in the absence of substrate (supplemental movies 1 and 2). Overall r.m.s. deviation between the two complexes is 0.51 Å and is almost the same (0.6 Å) for carboxyl residues anchoring desosamine. This indicates that specific substrate-anchoring modes largely account for the diversity of PikC products rather than an induced fit mechanism.

The two YC-17 hydroxylation sites, allylic C10 and methylene C12 atoms, are within 7.5 and 5.3 Å from the heme iron, respectively (Figs. 3*B* and 4*B*). However, the C12–C13 bond of YC-17 is rotated slightly away from the heme iron, thus presenting a C–H bond at C12 for catalysis. This favorable stereochemical arrangement in combination with the 5.3 Å distance to the heme iron apparently leads to hydroxylation of YC-17 at C12, giving rise to neomethymycin (Fig. 1). However, the question remains whether the C10 position in YC-17 is hydroxylated from this same binding orientation and/or via the same mechanism since it is separated by >7 Å from the heme iron atom.

Site-directed Mutagenesis in Desosamine Binding Pockets—To investigate directly the role of carboxyl functionalities in the desosamine binding pockets, site-directed mutagenesis was performed to replace Asp-50, Glu-85, and Glu-94 with alanine or glutamine/asparagines (Fig. 6). Functional activity of the mutant enzymes was assessed *in vitro*. Reaction products were analyzed by high pressure liquid chromatography. Substitution of the proximal carboxyl group forming a salt bridge to the C3′ dimethylamino group, Glu-94 for YC-17 and Glu-85 for narbomycin, almost entirely abolishes conversion of the corresponding substrate, indicating that both charge and hydrogen-bonding capacities in the proximal position are essential for desosamine anchoring. This result is in agreement with a stringent requirement of hydrogen-bonding functionality in the C3′ position in genetically modified sugars (14–17). Substitution of the carboxyl at distal amino acid groups (Glu-85 for YC-17 and Asp-50 for narbomycin) generated PikC mutants that retain partial to complete catalytic activity, indicating that the negative charge of the distal carboxyl is dispensable. Interestingly, the E85Q mutant, which lacks a negative charge but retains a hydrogen-bonding capability, shifts the product ratio of YC-17 hydroxylation toward methymycin (Fig. 6). This change in product profile does not rule out the possibility of interchangeable roles of proximal and distal carboxyl groups in desosamine binding, which may result in realignment of YC-17 in the active site, bringing C10 closer to the heme iron. Substitution of a third residue not partic-

ipating in binding, Asp-50 for YC-17 and Glu-94 for narbomycin, allows full (YC-17) or significant residual (narbomycin) conversion to occur. It is particularly interesting that the D50N mutant provides more efficient hydroxylation of both macrolide substrates when compared with native PikC. Double mutant E85A/E94A is catalytically incompetent toward both endogenous macrolactone substrates (not shown).

In summary, we have determined four x-ray structures for the PikC P450 monooxygenase that catalyzes hydroxylation of two macrolide substrates, leading to four dominant reaction products. Based on these data, a unique anchoring mechanism has been identified that involves a specific salt bridge of glutamate amino acid residues to the C3′ dimethylamino group of the deoxysugar substituent. Site-directed mutagenesis of Glu-85, Glu-94, and Asp-50 amino acid residues in the substrate binding pocket were conducted to confirm the role of each in desosamine anchoring and their impact on the product ratio. Formation of a salt bridge between the protein carboxyl group and desosamine dimethylamino group is essential for catalytic conversion of each substrate. The data suggest that substrate tolerance and diverse product distribution occur from two specific anchoring orientations rather than induced fit mechanisms. The 12- and 14-membered ring macrolactone portions of both macrolide substrates bind in the active site, utilizing virtually the same set of protein-substrate interactions. In contrast, the desosamine group binds in two alternative binding pockets, each providing two carboxyl residues, one of which involves a salt bridge to a C3′ dimethylamino group of desosamine. Moreover, the presence of two desosamine binding pockets provides a unique opportunity to develop rational design of unnatural glycosylated substrates for PikC. It also enables selection of one of the two desosamine binding sites by site-directed mutagenesis to shift reaction product distribution toward a single desirable bioactive metabolite. It is particularly intriguing that the "acceptor" carbon atoms are located in non-equivalent positions with respect to the heme iron. Based on the x-ray structure, there is a ~5 Å distance between the heme iron atom and the corresponding reactive methylene C atom that results in hydroxylation of analogous positions, C12 in YC-17, leading to neomethymycin, and C14 in narbomycin, leading to neopikromycin (Fig. 1). The latter hydroxylation product is formed in very low amounts, which might be due to the unfavorable stereochemistry of the C14–C15 bond that points toward the heme iron with both C14–H bonds directed away from the oxygen scission site. Two other analogous allylic hydroxylation sites, C10 in YC-17 and C12 in narbomycin, are both within 7.5 Å from the heme iron. This is far enough to raise questions about the ability of these positions to be hydroxylated (i) from this same substrate orientation as opposed to an alternative, as yet uncovered substrate orientation or (ii) via an oxo-ferryl P450 intermediate as opposed to a peroxy-iron species.

Acknowledgments—We thank Dr. Fred P. Guengerich and Dr. John H. Dawson for helpful discussions and SER-CAT, Argonne National Laboratory, for assistance with data collection.

REFERENCES

1. Retsema, J., and Fu, W. (2001) *Int. J. Antimicrob. Agents* **18,** Suppl. 1, S3–S10
2. Furneri, P. M., and Nicoletti, G. (1991) *J. Chemother.* **3,** Suppl. 1, 24–27
3. Goldman, R. C., and Scaglione, F. (2004) *Curr. Drug. Targets Infect. Disord.* **4,** 241–260
4. Hutchinson, C. R. (1998) *Curr. Opin. Microbiol.* **1,** 319–329
5. Baltz, R. H. (1998) *Trends Microbiol.* **6,** 76–83
6. Menzella, H. G., Reid, R., Carney, J. R., Chandran, S. S., Reisinger, S. J., Patel, K. G., Hopwood, D. A., and Santi, D. V. (2005) *Nat. Biotechnol.* **23,** 1171–1176
7. Reeves, C. D. (2003) *Crit. Rev. Biotechnol.* **23,** 95–147
8. Rix, U., Fischer, C., Remsing, L. L., and Rohr, J. (2002) *Nat. Prod. Rep.* **19,** 542–580
9. Ackermann, G., and Rodloff, A. C. (2003) *J. Antimicrob. Chemother.* **51,** 497–511
10. Yonath, A. (2005) *Mol. Cells* **20,** 1–16
11. Auerbach, T., Bashan, A., and Yonath, A. (2004) *Trends Biotechnol.* **22,** 570–576
12. Khosla, C., Gokhale, R. S., Jacobsen, J. R., and Cane, D. E. (1999) *Annu. Rev. Biochem.* **68,** 219–253
13. Yoon, Y. J., Beck, B. J., Kim, B. S., Kang, H. Y., Reynolds, K. A., and Sherman, D. H. (2002) *Chem. Biol.* **9,** 203–214
14. Zhao, L., Sherman, D. H., and Liu, H.-w. (1998) *J. Am. Chem. Soc* **120,** 10256–10257
15. Zhao, L., Que, N. L. S., Xue, Y., Sherman, D. H., and Liu, H.-w. (1998) *J. Am. Chem. Soc.* **120,** 12159–12160
16. Zhao, L., Ahlert, J., Xue, Y., Thorson, J. S., Sherman, D. H., and Liu, H.-W. (1999) *J. Am. Chem. Soc.* **121**
17. Borisova, S. A., Zhao, L., Sherman, D. H., and Liu, H.-w. (1999) *Org. Lett.* **1,** 133–136
18. Tang, L., and McDaniel, R. (2001) *Chem. Biol.* **8,** 547–555
19. Xue, Y., and Sherman, D. H. (2001) *Metab. Eng.* **3,** 15–26
20. Xue, Y., Wilson, D., Zhao, L., Liu, H.-w., and Sherman, D. H. (1998) *Chem. Biol.* **5,** 661–667
21. Lee, S. K., Park, J. W., Kim, J. W., Jung, W. S., Park, S. R., Choi, C. Y., Kim, E. S., Kim, B. S., Ahn, J. S., Sherman, D. H., and Yoon, Y. J. (2006) *J. Nat. Prod.* **69,** 847–849
22. Zhang, Q., and Sherman, D. H. (2001) *J. Nat. Prod.* **64,** 1447–1450
23. Omura, T., and Sato, R. (1964) *J. Biol. Chem.* **239,** 2379–2385
24. Otwinowski, Z., and Minor, W. (1997) *Methods Enzymol.* **276,** 307–326
25. Brunger, A. T., Adams, P. D., Clore, G. M., Delano, W. L., Gros, P., Grosse-Kunstleve, R. W., Jiang, J.-S., Kuszewski, J., Nilges, M., and Pannu, N. S. (1998) *Acta Crystallogr. Sect. D Biol. Crystallogr.* **54,** 905–921
26. Cupp-Vickery, J. R., and Poulos, T. L. (1995) *Nat. Struct. Biol.* **2,** 144–153
27. Jones, T. A., Zou, J. Y., Cowan, S. W., and Kjeldgaard, M. (1991) *Acta Crystallogr. Sect. A* **47,** 110–119
28. Laskowski, R. A., MacArthur, M. W., Moss, D. S., and Thornton, J. M. (1993) *J. Appl. Crystallogr.* **26,** 283–291
29. Yano, J. K., Koo, L. S., Schuller, D. J., Li, H., Ortiz de Montellano, P. R., and Poulos, T. L. (2000) *J. Biol. Chem.* **275,** 31086–31092
30. Park, S. Y., Yamane, K., Adachi, S., Shiro, Y., Weiss, K. E., Maves, S. A., and Sligar, S. G. (2002) *J. Inorg. Biochem.* **91,** 491–501
31. Scott, E. E., He, Y. A., Wester, M. R., White, M. A., Chin, C. C., Halpert, J. R., Johnson, E. F., and Stout, C. D. (2003) *Proc. Natl. Acad. Sci. U. S. A.* **100,** 13196–13201
32. Ravichandran, K. G., Boddupalli, S. S., Hasemann, C. A., Peterson, J. A., and Deisenhofer, J. (1993) *Science* **261,** 731–736
33. Hilal, S., Karickhoff, S. W., and Carreira, L. A. (1995) *Quant. Struc.-Act. Relat.* **14,** 348
34. Goldman, R. C., Fesik, S. W., and Doran, C. C. (1990) *Antimicrob. Agents Chemother.* **34,** 426–431
35. Schlunzen, F., Zarivach, R., Harms, J., Bashan, A., Tocilj, A., Albrecht, R., Yonath, A., and Franceschi, F. (2001) *Nature* **413,** 814–821
36. Hansen, J. L., Ippolito, J. A., Ban, N., Nissen, P., Moore, P. B., and Steitz, T. A. (2002) *Mol. Cell* **10,** 117–128

37. Schlunzen, F., Harms, J. M., Franceschi, F., Hansen, H. A., Bartels, H., Zarivach, R., and Yonath, A. (2003) *Structure* **11,** 329–338
38. Berisio, R., Schluenzen, F., Harms, J., Bashan, A., Auerbach, T., Baram, D., and Yonath, A. (2003) *Nat. Struct. Biol.* **10,** 366–370
39. Nagano, S., Li, H., Shimizu, H., Nishida, C., Ogura, H., Ortiz de Montellano, P. R., and Poulos, T. L. (2003) *J. Biol. Chem.* **278,** 44886–44893
40. Nagano, S., and Poulos, T. L. (2005) *J. Biol. Chem.* **280,** 31659–31663
41. Modi, S., Sutcliffe, M. J., Primrose, W. U., Lian, L. Y., and Roberts, G. C. (1996) *Nat. Struct. Biol.* **3,** 414–417
42. de Visser, S. P., Ogliaro, F., Sharma, P. K., and Shaik, S. (2002) *J. Am. Chem. Soc.* **124,** 11809–11826
43. Sono, M., Roach, M. P., Coulter, E. D., and Dawson, J. H. (1996) *Chem. Rev.* **96,** 2841–2888
44. Meunier, B., deVisser, S. P., and Shaik, S. (2004) *Chem. Rev.* **104,** 3947–3980
45. Chandrasena, R. E., Vatsis, K. P., Coon, M. J., Hollenberg, P. F., and Newcomb, M. (2004) *J. Am. Chem. Soc.* **126,** 115–126
46. Vaz, A. D. N., McGinnity, D. F., and Coon, M. J. (1998) *Proc. Natl. Acad. Sci. U. S. A.* **95,** 3555–3560
47. Jin, S., Makris, T. M., Bryson, T. A., Sligar, S. G., and Dawson, J. H. (2003) *J. Am. Chem. Soc.* **125,** 3406–3407
48. Anliker, R., Dvornik, D., Gubler, K., Heusser, H., and Prelog, V. (1956) *Helv. Chim. Acta* **39,** 1785–1790
49. Djerassi, C., and Halpern, O. (1957) *J. Am. Chem. Soc.* **79,** 3926–3928
50. Djerassi, C., Halpern, O., Wilkinson, D. I., and Eisenbraun, E. J. (1958) *Tetrahedron* **4,** 369–381